Princeton University
Mechanical & Aerospace Engineering

MAE 423
Heat Transfer

Investigating Simulated Convective Flow over a Cylinder and Golf Ball

Jonathan Melkun & Mohamed Hamza

Executive Summary

The goal of the project is to numerically simulate two-dimensional unsteady heat convection from bodies of arbitrary geometry. This involves the simulation of unsteady incompressible viscous flows with heat transfer at relatively low Reynolds numbers where three-dimensional effects may be negligible. The first body we examine is a isothermal circular cylinder with constant surface temperature of 400K which is placed within an unsteady flow of low Reynolds number 200. In addition, we made the temperature of the inflow and upper and lower 'free lids' at 300K. The fluid used in the simulation was dry air and having used MATLAB, the diameter of the cylinder was 50 grid points long. The spacing, denoted by variable h, was calculated given our upstream velocity of 0.1 meters per second. Knowing this allowed us to find the Reynolds number of the flow to be approximately 200, fitting the low Reynolds number range condition. Finally, with the finished simulation, vorticity, temperature and streamfunction values were animated, leading us to being able to plot both final temperature and velocities along the cylinder as well as the changes in temperature over time throughout the flow over a fixed region of space.

We followed the circular cylinder simulation with an investigation of a golf ball because we were interested in determining how the dimples in the typical golf ball design alter the convective flow around the body. The same conditions were used with the golf ball as was used with the round cylinder. To be specific, those conditions included the fluid in the simulation being dry air, the upstream velocity being 0.1 meters per second, and making the diameter of the golf ball just as big as the cylinder, 50 grid points. Just like with the cylinder, after the simulation was completed, vorticity, temperature and streamfunction values were animated, allowing us to plot final temperature and velocities along the golf ball as well as demonstrating how the temperature changed with time over different points of the golf ball.

Critical equations and models used in the creation of these simulations and plots are as follows: the flow around the bodies was determined by using a streamfunction-vorticity model and the thermal energy equation for two-dimensional heat diffusion was used to calculate temperatures. One important aspect of the models was the simulation of small time steps, which was possible with the use of the Courant-Fredrichs-Lewy condition. In relation to the streamfunction, every time step was reiterated until a convergence within our chosen ten percent error margin was achieved. The value of ten percent was elected because it created a balance between the accuracy and simulation computing speed.[1]

In total, our animations were 10 seconds long, meaning we used 6443 time steps. Examining the flow, we saw the phenomena called the Von Karman vortex street form. This vortex street can be defined as a repeating pattern of swirling vertices that appears in the wake of flows around a body. Once the vortex shedding occurred after the body, we saw that the flow in the golf ball investigation exhibited a similar pattern to that of the cylinder. The main differences are that the boundary layer stayed closer to the body and the vortex shedding occurred half a second earlier because the dimples in the golf ball induce turbulence earlier than in the case of the smooth circular cylinder.

[1] All equations and conditions are mentioned in the following section of this project report: Methodology

Methodology

In creating the simulations, animations and plots, we used a host of equations to help accurately calculate the values we needed for every time step and every position/grid point in our system. Before using any equations though, we adequately model the diffusion of vorticity, we base our grid spacing on the grid Reynolds number, which is Equation 1. For $Re_h < 10$ the diffusive processes are adequately captured and modeled and since heat also diffuses, we account for the thermal diffusivity, α. This results in a grid spacing h that is restricted by $Re_h < 10$ or $(U_{inf}\, h)/\alpha < 10$, depending on whichever one yields the smaller h value.

With the mesh and h variables known, we focus next on the boundary conditions in which we had free top and bottom lids along with a uniform inflow and constant velocity outflow. Having free lids in the setup means that ψ is constant and ω is zero. Analyzing the next boundary conditions we see that having a uniform inflow leads to $\psi = U_{inf}\, y$ + constant and having a constant velocity outflow means ω must be constant.

Having the boundary conditions set allows us to use the Courant-Fredrichs-Lewy condition to determine the maximum allowable timestep consistent with the numerical stability shown in Equation 4.

Next, we use the Poisson Equation to control the flow field. Initializing this flow, we set the $\omega(0) = 0$, in other words vorticity equals zero when time is zero. With finite-difference approximation for ψ, we numerically iterate to solve the Laplace equation until we come upon a field that converges to a 0.01 percent. With the field set, we then calculate psi using the Gauss-Seidel iteration. The F variable in the Equation 3 is defined as the over-relaxation factor and as widely recommended is set to 1.5 for faster convergence.

One detail that must be paid attention to is the wall vorticity. Calculated using the no-slip condition, we arrive to Equation 5, which has been simplified given that ψ is zero for the cylinder points and the fact that adding up the neighboring wall streamfunction values gives the w+1, also known as the one grid point from the wall, value.

After having the initial and boundary conditions established we advance the convective flow at all the interior ‘bulk’ grid points for the current time step n, where $t = n\Delta t$. In the first part of this, we advance the vorticity in the convective fluid and then calculate u using Equation 6 and v using Equation 7. Then we use a finite-difference approximation as shown in the set of equations from Equation 8 to Equation 11. With these calculations complete, we now update ψ by numerically solving the Poisson Equation using Gauss-Seidel, as shown in Equation 12, where we continue to use 1.5 for the over-relaxation parameter, F.

The outflow boundary condition, at the right side of the domain where $i = i_{max}$, is calculated using Equation 12. At the outflow, we assume that u and v are constant and in addition to these assumptions, we assume that the vorticity simply convects out of the computational domain:

$w_{i,j} = w_{i-1,j}$.

The final step is to update the temperature in the bulk flow. To update the temperature field we use the energy equation without the dissipation term, which is negligible at low Reynolds numbers. Initially we impose constant-temperature boundary conditions which simplifies the coding, along with an initial constant temperature field in the bulk fluid. As was before, the cylinder stays at a constant temperature of 400K while the flow is initialized at 300K for when time is zero. After the initialization is where the bulk temperature changes are calculated using a set of equations from Equation 13 to Equation 16.

Outside of the coding part of the project, finding Strouhal's number gives us a sense of the common characteristics of the flow. For example, high Strouhal numbers have oscillations that dominate the flow while low values have oscillations that are simply dominated by the fast-moving fluid. Typically the Strouhal number would be calculated using Equation 17 but instead we used the animations to find the period of oscillation of the vortex shedding. Such calculations and findings are demonstrated in the results section below.

With regards to the golf ball investigation, the shape of the ball was created by taking the original cylinder shape and placing 18 circles of radius 3 grid points around the edge of the cylinder. The positions of the dimples were hand placed, however the generation of the circles was the same algorithm as the one to generate the larger cylinder, just with a radius set to 3 instead of 25 grid points. Other than this change, all the steps taken to create the simulation and animations for the cylinder apply for the golf ball section of this project.

For reference, our full code can be found in the appendix of this report.

Equations Table

Equation 1

$Re = (U_{inf}\ h)/\ \nu$

Equation 2: Poisson Equation

$$\nabla^2\psi = -\omega$$

Equation 3: Gauss-Seidel iteration

$$\psi_{i,j}^{k+1} = \psi_{i,j}^{k} + \frac{F}{4}\left(\sum \psi_{neighbors} - 4\psi_{i,j}^{k}\right)$$

Equation 4

$$\Delta t \leq \frac{h}{U_{max}}$$

Equation 5

$$\omega_w = -2\frac{\sum \psi_{w,\,neighbors}}{h^2} = -2\,\frac{\psi_{w+1} - \psi_w}{h^2}$$

Equation 6

$$u_{i,j}^{n} = \frac{\psi_{up}^{n} - \psi_{down}^{n}}{2h}$$

Equation 7

$$v_{i,j}^{n} = \frac{\psi_{left}^{n} - \psi_{right}^{n}}{2h}$$

Equation 8

$$\omega_{i,j}^{n+1} = \omega_{i,j}^{n} + \Delta t\left[-\frac{\Delta(u\omega)^n}{h} - \frac{\Delta(v\omega)^n}{h} + \nu\nabla^2\omega_{i,j}^{n}\right]$$

Equation 9

$$\nabla^2\omega_{i,j}^{n} = \frac{\sum \omega_{neighbors} - 4\omega_{i,j}^{n}}{h^2}$$

Equation 10

$$\Delta(u\omega)^n = \begin{cases} (u\omega)^n_{\text{right}} - (u\omega)^n_{i,j}, & u_{i,j} < 0 \\ (u\omega)^n_{i,j} - (u\omega)^n_{\text{left}}, & u_{i,j} > 0 \end{cases}$$

Equation 11

$$\Delta(v\omega)^n = \begin{cases} (v\omega)^n_{\text{up}} - (v\omega)^n_{i,j}, & v_{i,j} < 0 \\ (v\omega)^n_{i,j} - (v\omega)^n_{\text{down}}, & v_{i,j} > 0 \end{cases}$$

Equation 12

$$\psi^{n+1}_{i,j} = 2\psi^n_{\text{left}} - \psi^n_{2\,\text{left}}$$

Equation 13

$$T^{n+1}_{i,j} = T^n_{i,j} + \Delta t\left[-u^n_{i,j}\frac{(\Delta T)^n_{i,j}}{h} - v^n_{i,j}\frac{(\Delta T)^n_{i,j}}{h} + \alpha\nabla^2 T^n_{i,j}\right]$$

Equation 14

$$\nabla^2 T^n_{i,j} = \frac{\sum T_{\text{neighbors}} - 4T^n_{i,j}}{h^2}$$

Equation 15

$$u^n_{i,j}(\Delta T)^n_{i,j} = \begin{cases} u^n_{i,j}(T^n_{\text{right}} - T^n_{i,j}), & u_{i,j} < 0 \\ u^n_{i,j}(T^n_{i,j} - T^n_{\text{left}}), & u_{i,j} > 0 \end{cases}$$

Equation 16

$$v^n_{i,j}(\Delta T)^n_{i,j} = \begin{cases} v^n_{i,j}(T^n_{\text{up}} - T^n_{i,j}), & v_{i,j} < 0 \\ v^n_{i,j}(T^n_{i,j} - T^n_{\text{down}}), & v_{i,j} > 0 \end{cases}$$

Equation 17

$$\text{St} = \frac{fL}{U_\infty}$$

Results & Analysis

Cylinder

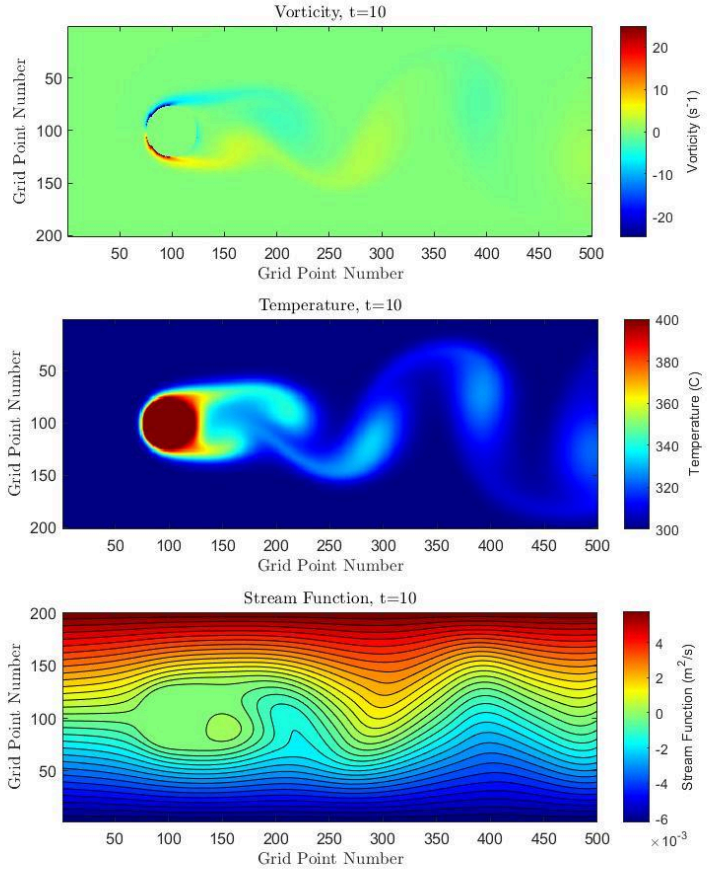

Figure 1: Final time step of the cylinder convective flow simulation

The simulation was run for a t_max of 10 seconds. The final time step is shown above. Note how the vortex shedding can be clearly seen in the vorticity, temperature, and stream function graphs. Vorticity on the cylinder is negative on the top and positive on the bottom, which corresponds to the flow curving toward the centerline after the cylinder. The temperature gradients are the most pronounced, with a range of 400K to 300K. The vortex shedding in the vorticity graph is less pronounced due to much higher vorticities on the left edge of the cylinder pulling up the color scale.

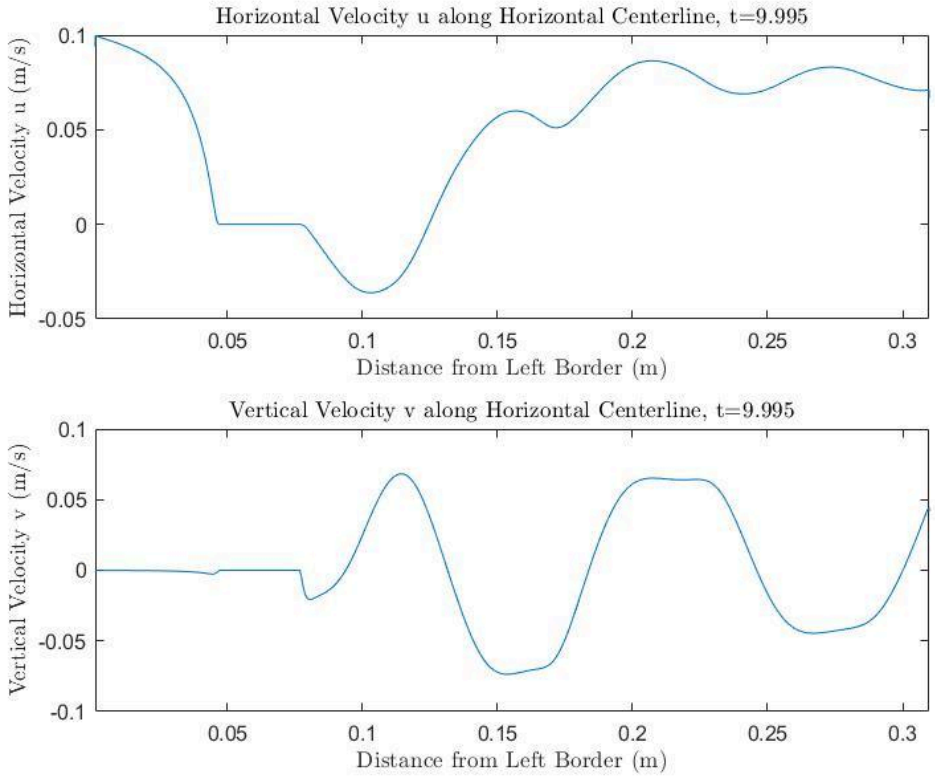

Figure 2: Plots of the horizontal and vertical components of velocity along the centerline of the simulation space

The horizontal and vertical components of the velocity, *u* and *v*, along the horizontal centerline are shown in the plots above. The plots show three distinct regions along the centerline: before the cylinder, later in the cylinder, and after the cylinder. The flow is initialized at 0.1m/s horizontally, which is shown in the graphs as u starts at 0.1 and v starts at 0. After the cylinder, the components enter a periodic fluctuation, which is characteristic of the vortex shedding present in the final time step. Another notable feature is that the horizontal velocity is almost always positive, which makes sense since the flow is moving to the right. The only region it is not positive is close to the right edge of the cylinder, where the low pressure region causes the air to move inwards, which corresponds to a negative *u*. The vertical component of velocity oscillates between positive and negative, which causes the vortices later in the flow to move up and down, as seen in the simulation.

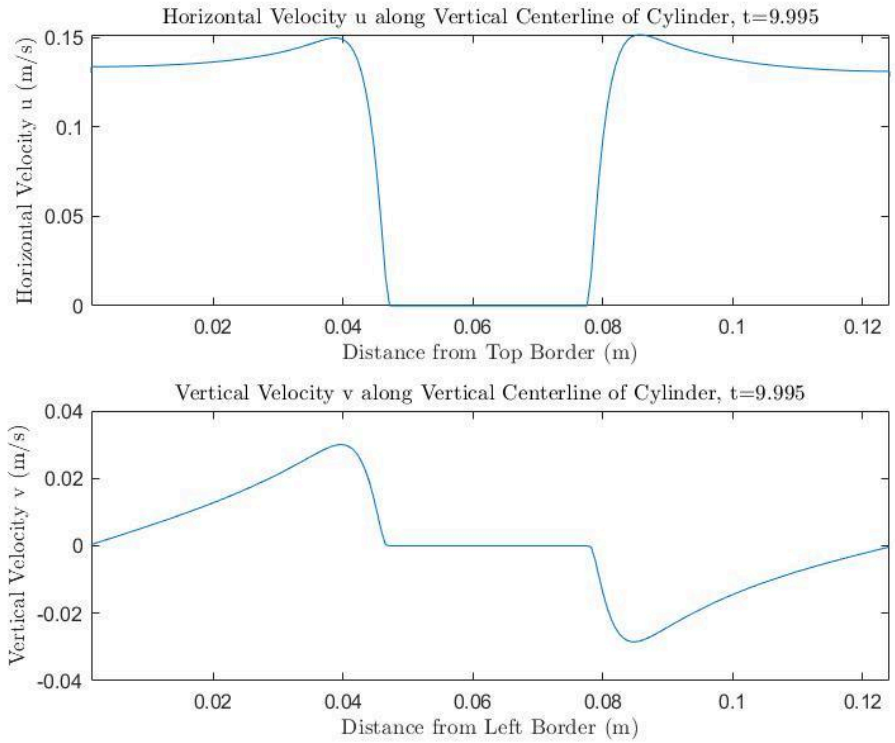

Figure 3: Plot of the horizontal and vertical components of velocity along the vertical centerline of the cylinder

The vertical centerline of the cylinder shows other aspects of the convective flow. The plot for u shows that the horizontal velocity speeds up as it gets closer to the cylinder, then drops to zero once it reaches the surface of the cylinder. The same is true for the vertical velocity graph, although the sign of the velocity is flipped on the right side of the cylinder since in order to move around the shape the flow must go up on the top half and down on the bottom half of the cylinder. This characteristic of the graphs arises due to the no slip condition being imposed on the surface of the cylinder, which makes the velocity zero on the surface of the cylinder. This also creates a small boundary layer around the cylinder, which can be seen around the graphs between the x values of about 0.04 and 0.05.

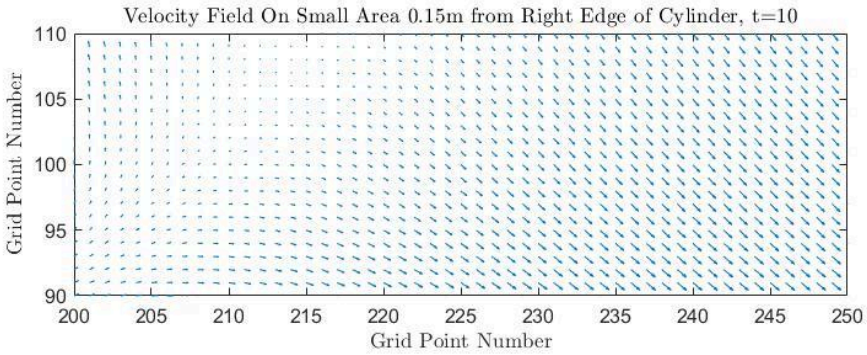

Figure 4: Velocity field of small area to the right of the cylinder. Arrow length corresponds to magnitude of velocity at that point.

A vector field of the velocity is shown above. This clearly shows how the velocity influences the direction of the flow, as the arrows moving up and down correspond to the shape and movement of the vortices.

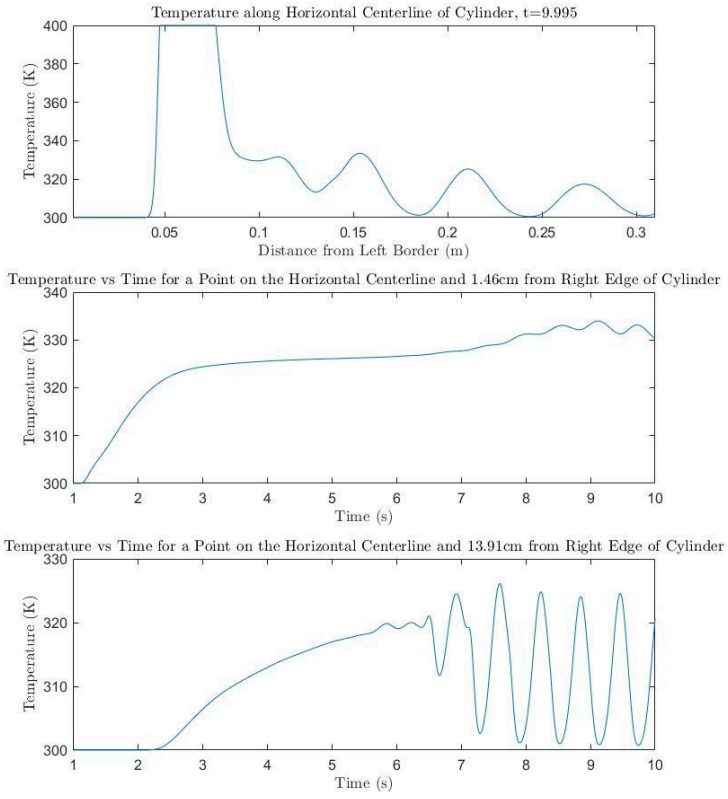

Figure 5: Various plots of temperature in the simulation. The first plot shows the temperature along the centerline for the final time step, while the other two plots show the evolution of temperature over the entire simulation for two points in the flow.

The temperature graph along the horizontal centerline shows the isothermal condition of 400K inside the cylinder as well as periodic temperature changes corresponding to vortex shedding. Two points, one close to the right edge of the cylinder and one farther away, were chosen to observe the oscillation of temperature over the simulation. The point close to the cylinder does show subtle oscillations, but it mainly stays around the 320-330K range. This is because the vortices start small closer to the cylinder, then grow in size as they move away from the cylinder.

The temperature graphs can also be used to indicate the heat flux coming out of the cylinder. Using the graph of the point 1.46 centimeters away from the cylinder, it is clear that the heat flux starts at zero, then increases to a high value as the flow is starting. Once the temperature flow progresses further to the right of the cylinder, the heat flux slows down. Once the vortices form and the temperature starts fluctuating, the heat flux also fluctuates. The heat flux on average stays positive throughout the simulation, indicating that the cylinder heat flux is generally positive and the cylinder is releasing energy. This makes sense, as the cylinder is at 400K and the surroundings are at 300K, so heat must be coming out of the cylinder.

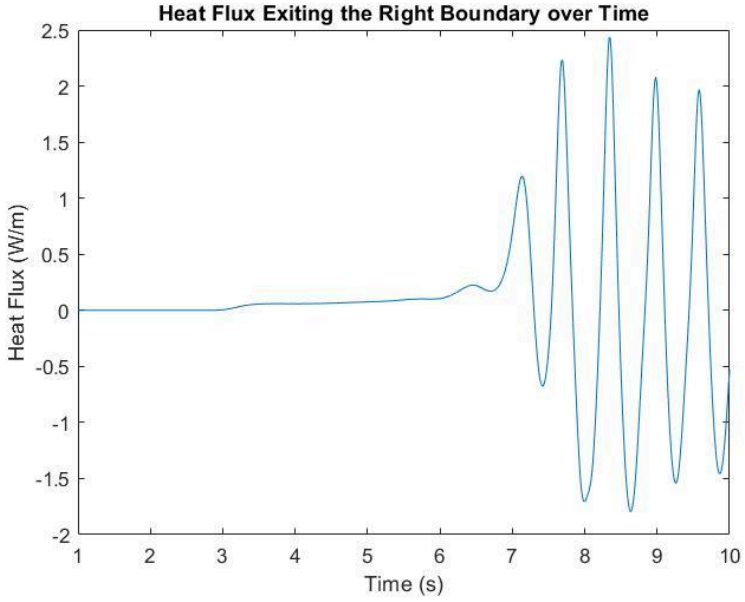

Figure 6: Plot showing the evolution of heat flux exiting the right boundary over time

The heat flow out of the right boundary was calculated throughout the 10 second simulation and is shown above. Using this, integrating the curve over time should produce the total energy that left the right boundary. Using MATLAB's cumtrapz function, this was found to be 31.72 J/m.

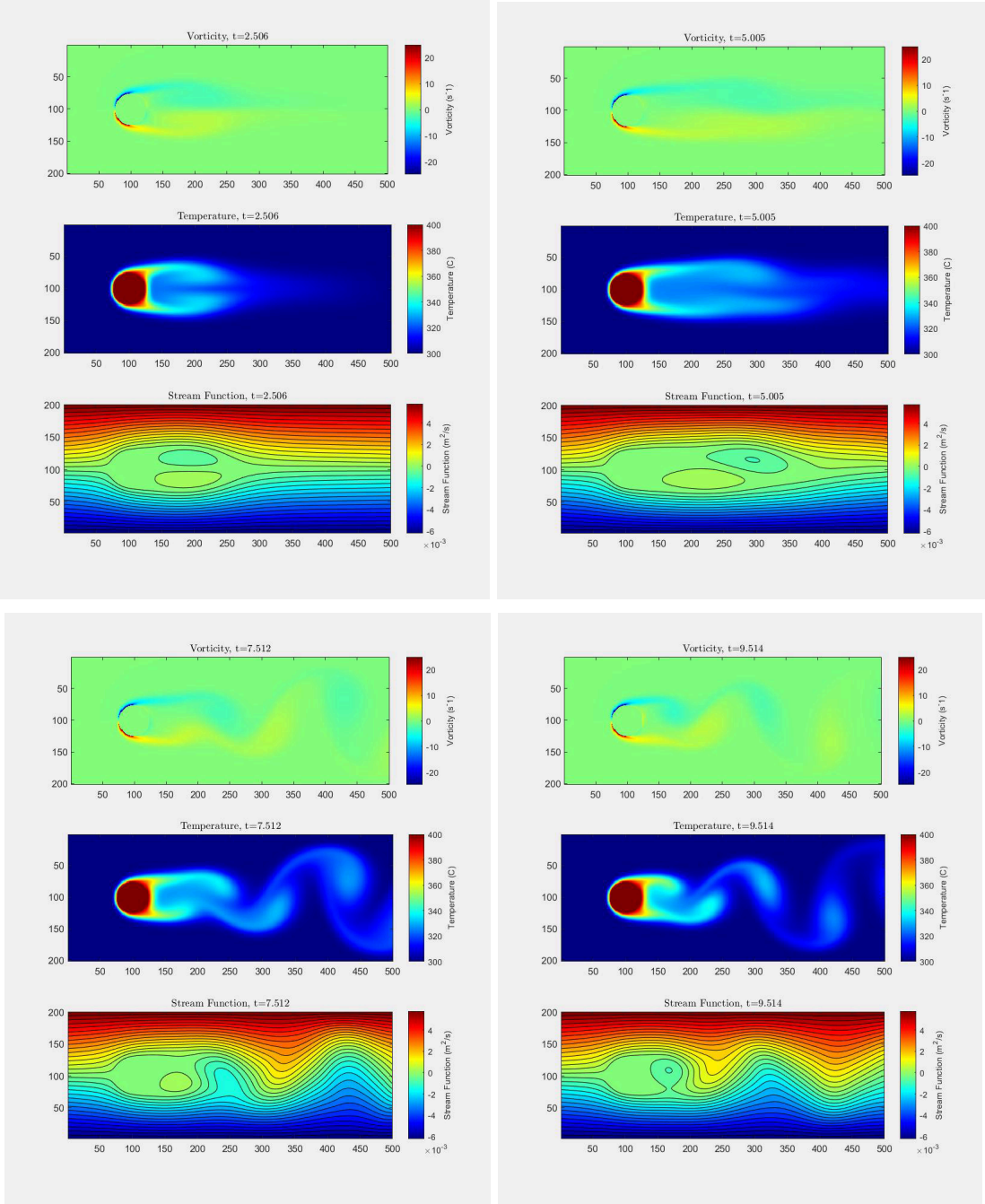

Figure 7: Four snapshots of the video of the simulation

Four snapshots of the video of the simulation shown above demonstrate the evolution of the flow over time. The flow starts relatively symmetrical, shown by the t = 2.5s snapshot. The flow can be seen curving in towards the centerline, but it is not until the t = 5s snapshot that the instability starts to form. By t = 7.5s, the vortex shedding becomes clear to see, and the t = 9.5s snapshot shows how the vortices continue to shed in a periodic fashion. The evolution is much more clearly seen in the avi video file included with the report submission.

To calculate the Strouhal number of the vortex shedding, the video of the temperature graph was used since it showed the clearest picture of the vortices. To find the period of oscillation of the vortices, the graph of t=7.069s was used as a starting point and the position of a current vortex was noted. Then the video was played until another vortex reached that same point and the difference in time was recorded by the title of the graphs. Through this method, the period of oscillation was estimated to be 1.568, which leads to a frequency of 0.638 Hz. Plugging this into Equation 17, with a radius of yields a Strouhal number of 0.198.

$$Sr(Re) = 0.2684 - \frac{1.0356}{\sqrt{Re}}.$$

*Equation 18: Strouhal Number as a function of Reynolds Number for 47<Re<2*10^5(Fey, König, and Eckelmann, 1998)*

Using Equation 18, with Re_D=200, a typical Strouhal number is 0.195. The Strouhal number we found is extremely close to the accepted value, giving us confidence in our simulation accuracy.

Golf Ball

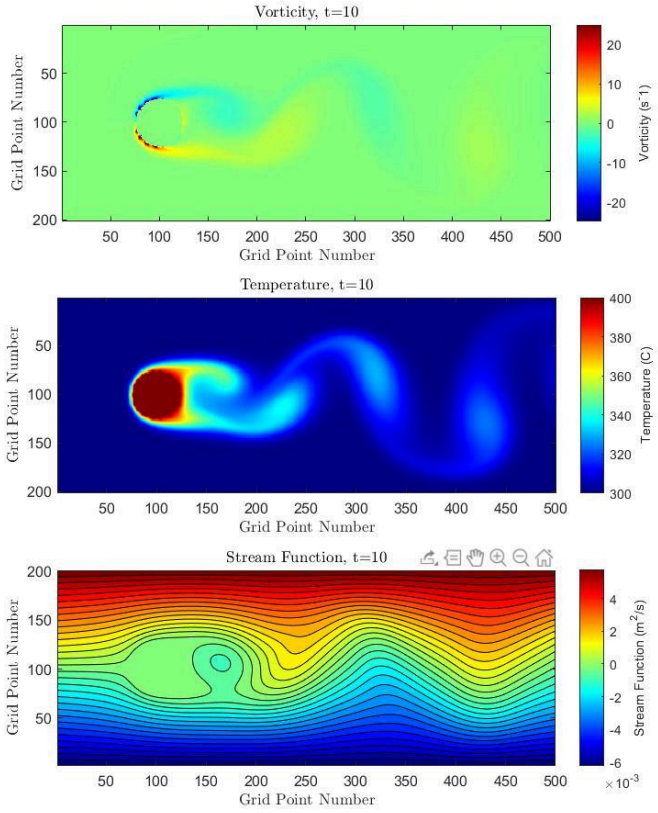

Figure 8: Final time step of the golf ball convective flow simulation

The figure above shows the final time step of the golf ball simulation. As all of the flow characteristics were kept the same as the cylinder, it is not unexpected that the flow exhibits similar characteristics of the cylinder simulation.

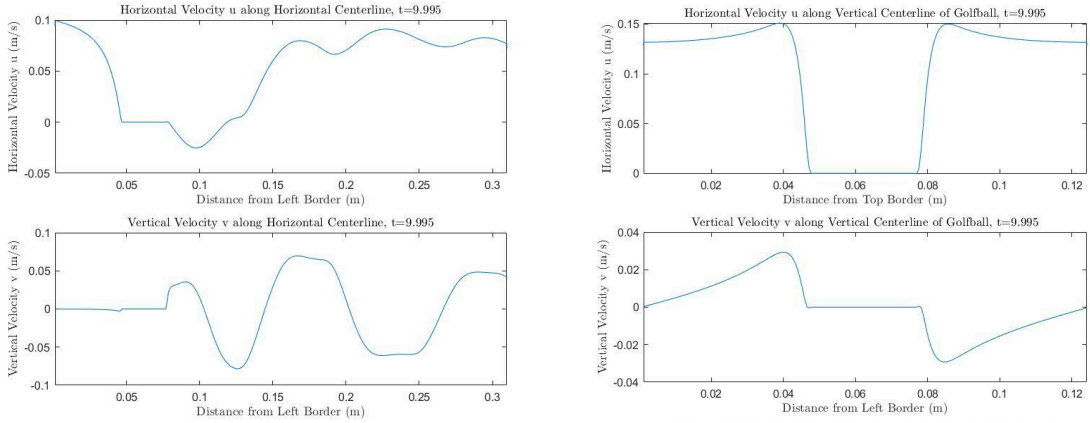

Figure 9: Velocity plots over the horizontal and vertical centerlines of the golf ball, analogous to the same plots of the cylinder flow

The graphs of the velocity components also share a similar shape to those of the cylinder simulation. The area close to the right edge of the cylinder shows a slight difference between the two flows. Both the horizontal and vertical velocities along the horizontal centerline reach higher peaks in this area than those of the cylinder flow. This may be indicative of the boundary layer staying tighter toward the surface of the golf ball, since the more aggressive velocity values may be keeping the flow closer to the circular shape of the surface rather than separating away from the surface.

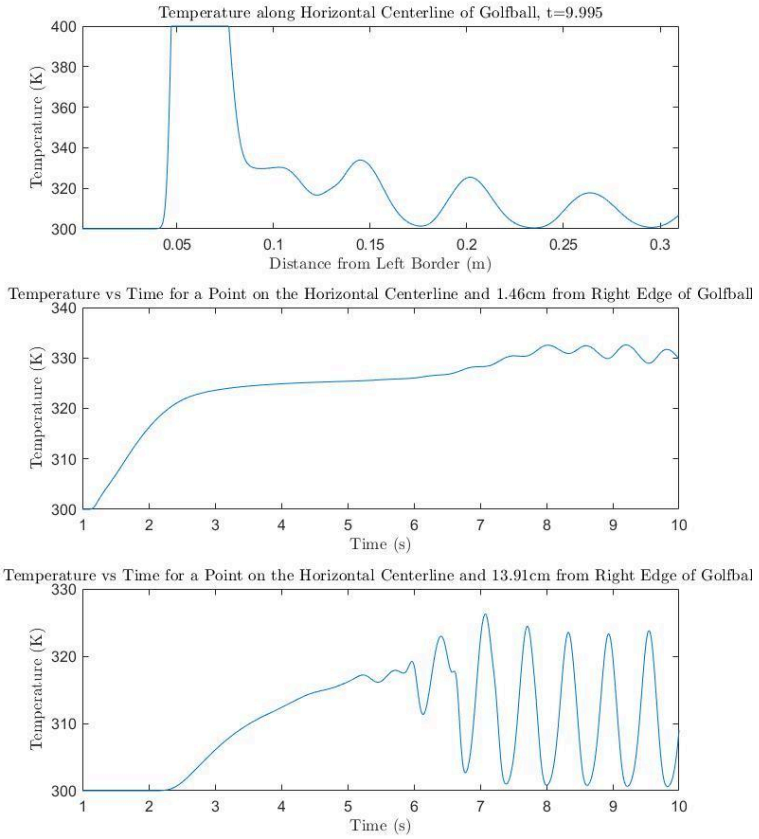

Figure 10: Various temperature graphs of the golf ball flow, analogous to those of the cylinder flow

The temperature vs time plots of the golf ball flow also show a difference between the golf ball and cylinder flows. From the graph of the point 13.91 centimeters away from the cylinder, the temperature oscillations start at around 6.1 seconds, while the oscillations in the cylinder flow start at around 6.6 seconds. This is measured by the first time the temperature drops. This shows that vortex shedding occurs about 0.5 seconds earlier with the golf ball shape than the smooth cylinder shape. The period of oscillation and in turn the Strouhal number however is nearly identical, it simply starts sooner.

Discussion & Conclusion

Part 1: Debugging

Points of conflict with the coding process of this project included getting the simulation to work past the first time step, which we resolved by fine tuning and sign adjustments in our indexing. Another major issue was having the code not recognize high temperature gradients Fixed by lowering Reynolds number and having a more conservative time step by assuming a max velocity of $4*U_{inf}$. These difficulties in coding stalled our progress for a significant amount of

time but once met with solutions, all the other coding tasks ran smoothly and we were able to analyze our simulations and animations.

Part 2: Results

The cylinder simulation results look successful, but there are some limitations with the code that should be mentioned. Due to time constraints, some compromises were made to speed up calculations which may have affected the accuracy of the results. The convergence error tolerance for the psi iteration was set to 0.1. Preliminary experimentation showed that decreasing the error tolerance any further did not produce visually different results, so this relatively low tolerance was selected for faster computation. It was also found that rather than calculating the distance every time to determine if a point was inside the cylinder or not, it was much faster and simpler to compute a boolean array which was set to true if it was inside the cylinder and false if it was outside the cylinder. This saved on having to calculate distance for every point inside the main time loop, and checking a simple boolean flag which was much quicker. Combined with a fast processor and these optimizations the code took around 40 minutes to produce 10 simulated seconds or around 6443 time steps.

The Strouhal number found from the simulation was very close to experimentally accepted values for a cylinder. This gives us confidence in the accuracy of our simulation as it can be verified by comparing it with real-world results. The heat transfer graph out of the right boundary, however, seems inaccurate, as the heat flux should almost always be positive since the cylinder is constantly emitting heat and that heat is being carried by the flow. This may be due to a coding error, but it still provides a qualitative view of how the energy being emitted by the cylinder changes throughout the flow. The heat flux speeds up and slows down periodically, which corresponds to the periodic vortex shedding.

The idea for the golf ball was inspired by topics from a previous fluid mechanics course, where we learned that the dimples in the golf balls reduce the drag on the ball by inducing turbulence and causing the boundary layer to stick better to the surface of the ball. We wanted to see if this theory would hold up in our simulation.

The golf ball shape was a challenge to represent in the code. Firstly, the code could only represent a two-dimensional flow, so the spherical shape had to be simplified to a circle. Also, due to time constraints and computational power, the resolution of 201 by 500 was too small to accurately represent the geometry of a golf ball. A typical golf ball has dimples that have a depth about 0.6% of the golf ball diameter. This would translate to less than a gridpoint in our cylinder, which was impossible. Therefore, we opted to use a shape inspired by a golf ball, with dimples much larger and deeper than a real ball. The resulting shape was quite jagged, but at least it was symmetrical. It also did not break the code most importantly, which earlier attempts did.

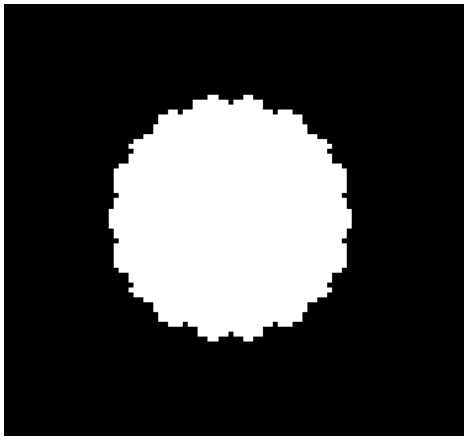

Figure 11: Image of “golf ball” shape

The objective was to see if the dimples would have an effect on the resulting flow, and in that sense the experiment was successful. As stated in the results section, the dimples in the ball produced a boundary layer that separated later in the flow and induced turbulent vortices earlier in time. This can be explained by the dimples producing small pockets of turbulence, which allows a greater diffusivity of energy in the boundary layer and allows the boundary layer to cling to the surface a little longer. It was interesting to see this theory applied practically in the simulation results and with visual clarity.

For future work, it would be interesting to increase resolution of the simulation to actually see the mini vortices forming in the dimples of the golf ball. Experimenting with different shape and sized dimples would be an additional future work that could possibly help explain why we use the modern-day golf ball design as opposed to some other shape design. On a bigger scale, investigating the aerodynamics of a sports car and pinpointing specific parts of the car like the front or rear wings for example and optimizing those would be excellent options for future work as it is based on our project slightly and has huge potential for financial success in the field of sports racing.